Behavior of depleted elastic networks: Comparison of effective-medium and numerical calculations

Lawrence M. Schwartz, Shechao Feng,* M. F. Thorpe,† and Pabitra N. Sen
Schlumberger-Doll Research, Old Quarry Road, Ridgefield, Connecticut 06877-4108
(Received 30 April 1985)

Machine simulations and effective-medium theories are used to examine the influence of transverse (i.e., noncentral) forces on the elastic percolation transition in two dimensions. We consider models in which the transverse forces arise from (1) contact interactions between pairs of macroscopic particles and (2) bond-bending forces involving three-site interactions. In the first class of models, effective-medium theory is shown to describe with surprising accuracy the dependence of the bulk and shear moduli on the bond occupation parameter p. In all cases we find that, as p is decreased, the ratio of the bulk to the shear modulus approaches a value that is independent of the system's initial parameters, but which does depend on the microscopic details of the model. Finally, we consider the description of depleted elastic systems from a continuum viewpoint. Two distinct effective-medium theories are shown to predict behavior consistent with that obtained in our microscopic analysis. Here, however, the ratio of the bulk to shear modulus at threshold varies over a continuous range of values.

I. INTRODUCTION

We present here the results of calculations based on both microscopic[1–9] and macroscopic[10–13] models of depleted elastic media. Our microscopic results are obtained by applying computer-simulation techniques and the effective-medium approximation (EMA) to a two-dimensional network. Our macroscopic work is based on generalizations of the EMA to the description of voids in continuous elastic media. As a whole our results offer strong evidence for the existence of fixed-point behavior in the vector-percolation problem. For any choice of the initial parameters specifying a give model, as the system is depleted, the ratio of the bulk modulus (K) to the shear modulus (μ) flows to a value that is *independent* of the parameters that characterize the undepleted system. While it was proposed that K/μ would approach a *universal* value at the depletion transition,[2] our finding that this value depends on the microscopic structure of the model is consistent with recent results of Bergman.[5]

Several authors have devoted their attention to the description of tenuous elastic media.[1–9,13–20] A particularly interesting example is a lattice of interacting particles in which a fraction, p, of the bonds have been removed at random. As p decreases, the system's elastic moduli decrease and eventually vanish to a critical value, p_c^*. If the interparticle forces are purely central, it is known that the value of p_c^* is significantly higher than the corresponding value, $p_c^{\rm cond}$, for the electrical conductivity threshold.[1] In most materials of physical interest, however, there are both central and noncentral forces[21–23] and it is important to understand the behavior of depleted elastic systems under more general conditions.[1–5]

An outline of this paper is as follows. In Sec. II A we introduce two microscopic models that will be studied in detail, by both effective-medium theory and computer simulation. The first model is a two-dimensional version of the granular system discussed by Schwartz *et al.*[23] Here the interacting "particles" are disks whose motion has both rotational and translational components. The second model is based on the standard Kirkwood bond-bending interaction.[21] A brief summary of our numerical methods is given in Sec. II B. In Sec. II C a sequence of techniques is employed to study the disk model. We begin by reviewing simple constraint-counting arguments[8,15] that can be used to estimate the value of p_c^*. We then consider effective-medium theories that allow us to compute the properties of the system over the entire range of p values. Both static[24] and dynamic[25] arguments are shown to lead to the same effective-medium equations. Interestingly, we find that the value of p_c^* implied by the effective-medium equations and that obtained from the constraint-counting arguments are *identical* in all cases. (While this finding is consistent with the work of other authors,[15,19] to our knowledge the reason for this agreement is not properly understood.) In the last part of Sec. II C, the results of effective-medium theory are compared with those obtained by numerical simulation. Three features of this comparison deserve comment. First, in all cases, the value of p_c^* obtained numerically agrees quite well with its effective-medium counterpart. Second, we find that the overall behavior of $K(p)$ and $\mu(p)$ as given by the simulations is in very good agreement with the effective-medium calculations. Third, both the numerical and effective-medium calculations indicate that the ratio K/μ approaches a fixed point as $p \to p_c^*$. As expected, however, the limiting value of K/μ is *not* given with any accuracy by effective-medium theory. (Physically, behavior at the transition point is dominated by long-range correlations which are inherently beyond the scope of effective-medium theory.) In Sec. II D the results of numerical simulations on the bond-bending model are discussed. For this system $p_c^* = p_c^{\rm cond}$ and we again find that K/μ approaches a fixed point as $p \to p_c^*$. However, in

this case there is no satisfactory generalization of the effective-medium equations developed in Sec. II C. In Sec. III we consider the effective-medium description of depleted elastic systems from a *continuum* viewpoint.[10–13] (No simulations have been done in this case.) Here the depletion is obtained by the creation of elliptical voids. Two effective-medium theories are discussed, both of which lead to fixed-point behavior at their respective transition points.[13] However, the limiting value of K/μ depends on the aspect ratio of the voids and varies over a continuous range of allowed values.

II. MICROSCOPIC MODELS

A. General considerations

When transverse (i.e., noncentral) forces are included in microscopic calculations, care must be taken to guarantee that the model is rotationally invariant.[1,22,23] (This requirement rules out the point mass nearest-neighbor model originally proposed by Born and Huang.[26]) We consider here two dynamical models. In both cases, the underlying lattice is taken to be a two-dimensional triangular network [with basis vectors: $\mathbf{a}_1=a\hat{\mathbf{e}}_x$ and $\mathbf{a}_2=a(\hat{\mathbf{e}}_x+\sqrt{3}\hat{\mathbf{e}}_y)/2$]. This network has the attractive feature that the long-wavelength sound speeds are *isotropic* (i.e., only two elastic constants are required to describe the system). The first model is a two-dimensional version of the model developed in Ref. 23. Here disks, with mass M, moment of inertia I, and radius $R=a/2$, are placed at each lattice site. The Hamiltonian is

$$H=\frac{1}{2}\sum_i\left[M\left[\frac{d}{dt}\delta\mathbf{u}_i\right]^2+I\left[\frac{d}{dt}\delta\theta_i\right]^2\right]+\frac{1}{4}\sum_{i\neq j}g_{ij}\{D_\perp[(\delta\mathbf{u}_i-\delta\mathbf{u}_j)-\frac{1}{2}(\delta\theta_i+\delta\theta_j)\hat{\mathbf{e}}_z\times\mathbf{R}_{ij}]^2$$
$$+(D_{||}-D_\perp)[(\delta\mathbf{u}_i-\delta\mathbf{u}_j)\cdot\mathbf{R}_{ij}]^2+D'(\delta\theta_i-\delta\theta_j)^2\}\ , \tag{2.1}$$

where $\mathbf{R}_{ij}\equiv\mathbf{R}_i-\mathbf{R}_j$ are lattice vectors, $\hat{\mathbf{e}}_z$ is a unit vector in the z direction (i.e., normal to the plane of the disks), and g_{ij} is a random variable with probability p of being unity and probability $1-p$ of being zero. Translational and rotational degrees of freedom associated with the ith site are represented by $\delta\mathbf{u}_i$ and $\delta\theta_i$, respectively; the quantities $D_{||}$ and $D_\perp$ monitor forces associated with the *relative* displacement of adjacent contact points. (The strength of the transverse interaction is monitored by the dimensionless parameter $d\equiv D_\perp/D_{||}$.) The parameter D' represents a torque that opposes the counter-rotation of adjacent grains in which there is no relative displacement of their contact points. This last coupling constant was not employed in Ref. 23, but terms of this kind are to be expected in more general situations.

In Eq. (2.1) the transverse forces are associated with the finite spatial extent of the individual particles (i.e., the disks). In a second model of interest the particles are point masses and the transverse forces are due to bond bending:[21,22]

$$H=\frac{1}{2}\sum_i M\left[\frac{d}{dt}\delta\mathbf{u}_i\right]^2+\frac{D_{||}}{2}\sum_{i\neq j}g_{ij}[(\delta\mathbf{u}_i-\delta\mathbf{u}_j)\cdot\hat{\mathbf{R}}_{ij}]^2$$
$$+\frac{D_\perp}{2}\sum_{\langle jik\rangle}g_{ij}g_{ik}[(\delta\mathbf{u}_i-\delta\mathbf{u}_j)\times\hat{\mathbf{R}}_{ij}$$
$$-(\delta\mathbf{u}_i-\delta\mathbf{u}_k)\times\hat{\mathbf{R}}_{ik}]^2\ . \tag{2.2}$$

Here $\langle jik\rangle$ indicates that the sum is over all triplets in which the bonds j—i and i—k form an angle whose vertex is centered at site i.

It should be emphasized that both of the above models are rotationally invariant. In the first model the particles have internal degrees of freedom but interact by nearest-neighbor (i.e., contact) forces. By contrast, in the second model, a change of bond angle involves the coupling of both second and third neighbors. If the rotational degrees of freedom are neglected in Eq. (2.1), we obtain the familiar Born model[26]

$$H=\frac{1}{2}\sum_i M\left[\frac{d}{dt}\delta\mathbf{u}_i\right]^2$$
$$+\frac{1}{4}\sum_{i\neq j}g_{ij}\{D_\perp[(\delta\mathbf{u}_i-\delta\mathbf{u}_j)\times\mathbf{R}_{ij}]^2$$
$$+(D_{||}-D_\perp)[(\delta\mathbf{u}_i-\delta\mathbf{u}_j)\cdot\hat{\mathbf{R}}_{ij}]^2\}\ . \tag{2.3}$$

It is well known that this Hamiltonian is *not* rotationally invariant.[22] Nevertheless, we will see that several important features of the percolation transition can be understood in terms of the Born model which has the advantage of being considerably simpler from a computational standpoint. (This model is also of interest in connection with the description of gels.[7])

B. Machine simulations

The computer simulations presented here employ standard relaxation methods.[27] Calculations have been carried out on 30×30 and 40×40 two-dimensional triangular lattices. (Results presented in this paper are based on the 30×30 system; the larger lattice was used to check the reliability of these calculations.[28]) In each simulation (i.e., for each value of p) the boundary sites of the lattice are given fixed displacements corresponding to either pure compression or pure shear (see Fig. 1). (Note that there is *no net torque* associated with the shear displacements.) The sites inside the boundary are then allowed to respond according to the equations of motion:

$$\delta\mathbf{u}_i(t_{n+1})=\delta\mathbf{u}_i(t_n)+\gamma\mathbf{F}_i(t_n)\ , \tag{2.4}$$

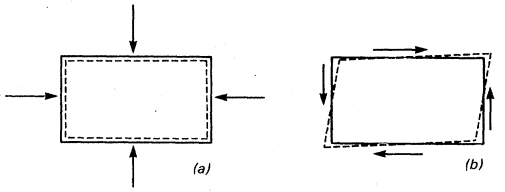

FIG. 1. Boundary displacements for determining (a) bulk and (b) shear moduli by numerical simulation are represented schematically. Note that the shear displacements do no involve any net torque.

where t_n is the nth time step, $\mathbf{F}_i(t_n)$ is the force on the ith particle at time t_n as calculated from the Hamiltonian and the boundary condition, and γ is a factor chosen to optimize the overall relaxation process. The iteration of Eq. (2.4) is terminated when the maximum force on each of the interior particles is smaller than a preset value ϵ. (A typical value in the present calculations is $\epsilon=0.01$.) The net forces on the boundary sites are then used to compute the elastic constants (K or μ). Having determined the displacements for a given value of p, these $\delta\mathbf{u}_i$ are used to set the initial conditions for the next p, which is obtained by randomly eliminating a specified number of bonds. This procedure is repeated until the elastic constants of the system approach zero. The entire process is executed 20 times (i.e., with 20 bond-removal sequences) to obtain the statistically averaged results presented in this article.

C. Nearest-neighbor (contact) forces

1. *Constraint counting*

To begin, we consider just the Born model defined by Eq. (2.3). Although we will soon specialize to the case of a triangular lattice, it is instructive to make the present arguments somewhat more generally. Suppose that a fraction, $1-p$, of the bonds are cut. The simplest way to estimate where the transition will take place is to use an argument based on the counting of zero-frequency modes.[8] For a system of N particles in two spatial dimensions, we have $2N$ vibrational degrees of freedom. There are two constraints (i.e., two kinds of motion that cost energy) associated with each bond. The number of zero-frequency modes is equal to the difference between the number of degrees of freedom and the number of constraints. The fraction of these modes is then

$$f=\frac{2N-\frac{1}{2}(2NZ)p}{2N}=1-\frac{Zp}{2}\ , \tag{2.5}$$

TABLE I. Illustration of the fact that Zp_c is nearly independent of a lattice in two dimensions.

Lattice	Z^* (Effective-medium theory)	Zp_c (Exact)
Honeycomb	2	2.0838
Square	2	2
Triangular	2	1.9581

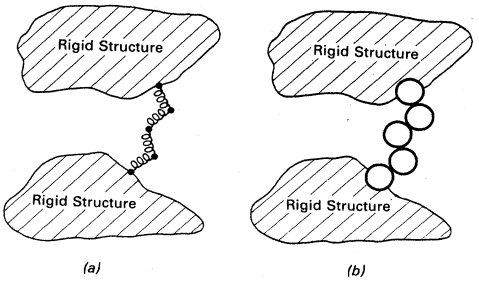

FIG. 2. Schematic illustration of the zero-frequency modes in (a) the central-force model and (b) the disk model with $D'=0$.

where Z is the number of neighbors. The transition sets in at $f=0$, i.e., when the lattice becomes rigid against all deformations. Thus

$$p^*=\frac{2}{Z}\ . \tag{2.6}$$

[Here p^* is to be understood as the constraint counting (or effective-medium) estimate for the true threshold p_c^*.] We emphasize that Eq. (2.5) is valid only for $p\le p^*$, clearly, negative values of f are meaningless.[8] This result is identical to the constraint-counting estimate[24] of the geometrical percolation threshold $p_c^{\rm cond}$ (see Table I). Alternatively, the transition can be viewed in terms of the mean coordination number $\langle Z\rangle\equiv pZ$. At the transition, $\langle Z\rangle\to Z^*=2$ (in two dimensions). (Note that Z^* is *independent* of Z.)

The preceding arguments can, of course, be used in the limit $D_\perp\to 0$ (i.e., central forces). In this case there is only one constraint per bond and we find $p^*=4/Z$ and $Z^*=4$. As expected, the inclusion of transverse forces shifts the threshold to significantly lower values.[1]

Consider next, the two-dimensional disk model. Here we have three degrees of freedom per site. If the parameter D' is set equal to zero, there are again two constraints associated with each bond, and the analog of Eq. (2.5) is

$$f=\frac{3N-\frac{1}{2}(2NZ)p}{3N}=1-\frac{Zp}{3}\quad (D'=0)\ . \tag{2.7}$$

The transition occurs at $p^*=3/Z$ and the corresponding value of $\langle Z\rangle$ is $Z^*=3$. Note that in this case the transition has shifted to a point exactly halfway between the central-force value, $p^*=4/Z$, and the Born-model result, $p^*=2/Z$. Physically this shift is associated with zero frequency (i.e., floppy) modes which involve chainlike sections of the percolating cluster. These modes involve no energy cost because, in the case $D'=0$, counter-rotation does not lead to any deformation of the contacts (see Fig. 2). Indeed, in Ref. 23 it is shown that in the case of one-dimensional systems (which form the tenuous links in the

TABLE II. Representative values of Z^*

	Central forces	Disk model ($D'=0$)	Disk model ($D'\neq 0$)
$d=2$	4	3	2
$d=3$	6	4	2

percolating cluster[3]) there are a macroscopic number of zero-frequency modes.

In the general case ($D'\neq 0$), the number of constraints acting at each contact increases from 2 to 3 and the fraction of zero-frequency modes is

$$f=\frac{3N-\frac{3}{2}(NZp)}{3N}=1-\frac{Zp}{2}\ . \tag{2.8}$$

The transition occurs at $p^*=2/Z$ or, equivalently, $Z^*=2$. In the present case, as in the Born model, p^* reduces to the corresponding estimate for the bond-percolation threshold $p_c^{\rm cond}$. This is reasonable because, with $D'\neq 0$, there are no displacements of two particles in contact that do not involve a cost in energy, and the transition takes place at the geometrical percolation limit.

The results of the preceding discussion can be expressed in terms of Z^*, a quantity we have seen is independent of the lattice. In the case of ordinary bond percolation, Kirkpatrick[24] has noted that Zp_c is *almost* a dimensional invariant. This point is illustrated in Table I. We see that the near universality of Z^* extends to the disk and central-force models for depleted elastic networks. The values of Z^* obtained in the various models are summarized in Table II.

For the triangular lattice studied in the remainder of this paper, the values p^* given by the constraints argument are $\frac{2}{3}$ (central-force model), $\frac{1}{2}$ (disk model with $D'=0$), and $\frac{1}{3}$ (Born model and disk model with $D'\neq 0$). We will see that these are exactly the values predicted by the effective-medium theories to be discussed in the following section. The central-force result $\frac{2}{3}$ is very close to the value in the numerical simulations. (Early calculations gave the value $p_c=0.58$,[1] but more recent estimates are much closer to $\frac{2}{3}$.[15,16]) The result $\frac{1}{3}$ is quite close to the value 0.3473 that is expected for bond percolation on a triangular lattice. We note that the numerical simulations for the disk model with $D'=0$ show that $p^*=\frac{1}{2}$ is a very good estimate for the triangular lattice.

To conclude this discussion, we note that for the bond-bending model the values of p_c^* and $p_c^{\rm cond}$ are expected to coincide. The model Hamiltonian (2.2) is locally rigid (i.e., all distortions of the depleted network involve a cost in energy).

2. *Effective-medium theory and simulations*

a. Static approach. In this section we develop effective-medium theories for the various models just discussed, by extending arguments first derived by Kirkpatrick[24] for depleted electrical networks. For simplicity, this approach will be illustrated for the Born model; results for the disk models will simply be summarized. The central approximation is to assume that a depleted network can be thought of as an effective *uniform* network with bond-strength parameters $\Delta_{||}$ and $\Delta_\perp$. These so called effective-medium bond strengths are determined by requiring that the fluctuations produced by replacing a selected effective bond by its actual value average to zero. In the present case this condition must be satisfied for external stresses corresponding to both compression and shear (recall Fig. 1).

Consider first the boundary condition associated with uniform compression. If every bond is described by $\Delta_{||}$ and $\Delta_\perp$, then it is clear that every bond is compressed by the same amount $\delta u_{\rm eff}$. Now imagine that bond 1—2 is replaced by one with strength $\tilde{D}_{||}$. It is evident that an extra compression $\delta\tilde{u}$ will result. To compute $\delta\tilde{u}$, we argue that restoration of the uniform strain situation would require the application of the force

$$\tilde{f}=\delta u_{\rm eff}(\Delta_{||}-\tilde{D}_{||})\ , \tag{2.9}$$

across (and in the direction of) the bond 1—2. Alternatively, by virtue of superposition principle, in the *absence* of any external pressure, the displacement associated with the force $\tilde{f}$ is simply $\delta\tilde{u}$. We then have

$$\tilde{f}=\delta\tilde{u}(\tilde{D}_{||}-\Delta_{||}+D_{||}^{\rm eff})\equiv\delta\tilde{u}\left[\tilde{D}_{||}-\Delta_{||}+\frac{\Delta_{||}}{a_{||}}\right]\ , \tag{2.10}$$

where $D_{||}^{\rm eff}\equiv\Delta_{||}/a_{||}$ is the ratio of $\tilde{f}$ to $\delta\tilde{u}$ when the system is ordered, i.e., when the bond 1—2 has the same strength as the rest of the bonds. Since $a_{||}$ is a property of the ordered system characterized by $\Delta_{||}$ and $\Delta_\perp$, it can be calculated exactly. The result is

$$a_{||}=\frac{2}{NZ}\sum_{\mathbf{k}}{\rm Tr}[\underline{\Delta}_{||}(\mathbf{k})\cdot\underline{\Delta}^{-1}(\mathbf{k})]\ , \tag{2.11}$$

where

$$\begin{aligned}\underline{\Delta}(\mathbf{k})&\equiv\sum_{\boldsymbol{\delta}}[1-\exp(i\mathbf{k}\cdot\boldsymbol{\delta})][\Delta_{||}\hat{\boldsymbol{\delta}}\hat{\boldsymbol{\delta}}+\Delta_\perp(\underline{\mathbb{1}}-\hat{\boldsymbol{\delta}}\hat{\boldsymbol{\delta}})]\\&\equiv\underline{\Delta}_{||}(\mathbf{k})+\underline{\Delta}_\perp(\mathbf{k})\ ,\end{aligned} \tag{2.12}$$

is the k-space dynamical matrix for our effective uniform medium, and $\boldsymbol{\delta}$ is a nearest-neighbor vector. Once $a_{||}$ is known, we have

$$\delta\tilde{u}=\delta u_{\rm eff}(\Delta_{||}-\tilde{D}_{||})\left[\frac{\Delta_{||}}{a_{||}}-\Delta_{||}+\tilde{D}_{||}\right]^{-1}\ . \tag{2.13}$$

The next step is to average over the two possibilities $\tilde{D}_{||}=D_{||}$ (probability p) and $\tilde{D}_{||}=0$ (probability $1-p$). Requiring $\langle\delta\tilde{u}\rangle\to 0$, we have

$$\frac{\Delta_{||}}{D_{||}}=\frac{p-a_{||}}{1-a_{||}}\ . \tag{2.14a}$$

The entire procedure described above can be applied to the case of an external shear-boundary condition to give the second effective-medium equation:

$$\frac{\Delta_\perp}{D_\perp}=\frac{p-a_\perp}{1-a_\perp}\ , \tag{2.14b}$$

where

$$a_\perp=\frac{2}{NZ}\sum_{\mathbf{k}}{\rm Tr}[\underline{\Delta}_\perp(\mathbf{k})\cdot\underline{\Delta}^{-1}(\mathbf{k})]\ . \tag{2.15}$$

Equations (2.11), (2.14), and (2.15) form a closed system of equations that determine $\Delta_{||}$ and $\Delta_\perp$. It is interesting to observe that

$$a_{||}+a_\perp\equiv\frac{2}{NZ}\sum_{\mathbf{k}}\sum_{\boldsymbol{\delta}}{\rm Tr}[\underline{\Delta}(\mathbf{k})\cdot\underline{\Delta}^{-1}(\mathbf{k})]\equiv\frac{4}{Z}\ . \tag{2.16}$$

Now, at the depletion threshold p_c^*, both $\Delta_{||}$ and $\Delta_\perp$ approach zero, and it follows from Eqs. (2.14) that $a_{||}^*=p_c^*=a_\perp^*$. This result together with (2.16) yields

$$p^*=2/Z \ . \tag{2.17}$$

which is identical to the result (2.6) obtained by the constraint counting argument. (A more detailed version of this argument is given in Ref. 15 for the case of *central* forces; their results are $a_\perp=0=\Delta_\perp$ and $p^*=4/Z$.)

The above analysis can easily be generalized to the two-dimensional disk models. Here the effective lattice is specified by three parameters $\Delta_{||}$, $\Delta_\perp$, and Δ', whose values are determined by the self-consistency conditions. Since we have one more degree of freedom in this case, the effective dynamical matrix $\underline{\Delta}(\mathbf{k})$ is a 3×3 matrix indexed by x, y, and θ:

$$\Delta_{\alpha\beta}(\mathbf{k})=\sum_{\delta}(1-e^{i\mathbf{k}\cdot\boldsymbol{\delta}})[\Delta_{||}\hat{\delta}\hat{\delta}+\Delta_\perp(\underline{1}-\hat{\delta}\hat{\delta})] \ , \tag{2.18a}$$

$$\Delta_{\alpha\theta}(\mathbf{k})=-\sum_{\delta}(1-e^{i\mathbf{k}\cdot\boldsymbol{\delta}})\Delta_\perp R(\hat{\mathbf{e}}_z\times\hat{\delta})_\alpha \ , \tag{2.18b}$$

$$\Delta_{\theta\alpha}(\mathbf{k})=-\sum_{\delta}(1-e^{i\mathbf{k}\cdot\boldsymbol{\delta}})\Delta_\perp R(\hat{\mathbf{e}}_z\times\hat{\delta})_\alpha \ , \tag{2.18c}$$

and

$$\Delta_{\theta\theta}(\mathbf{k})=\sum_{\delta}[\Delta_\perp R^2(1+e^{i\mathbf{k}\cdot\boldsymbol{\delta}})+\Delta'(1-e^{i\mathbf{k}\cdot\boldsymbol{\delta}})] \ , \tag{2.18d}$$

where $R=a/2$ is the disk radius, and α and β denote an arbitrary Cartesian index (x or y). Arguments similar to those presented above lead to the following results:

(i) $D'=0$. The structure of the final equations is the same as that of Eqs. (2.14). The quantities $a_{||}$ and $a_\perp$ are defined as

$$a_{||}=\frac{2}{NZ}\sum_{\mathbf{k}}\mathrm{Tr}[\underline{\Delta}(\mathbf{k}\mid\Delta_{||},\Delta_\perp=0,\Delta'=0)\cdot\underline{\Delta}^{-1}(\mathbf{k}\mid\Delta_{||},\Delta_\perp,\Delta'=0)] \tag{2.19a}$$

and

$$a_\perp=\frac{2}{NZ}\sum_{\mathbf{k}}\mathrm{Tr}[\underline{\Delta}(\mathbf{k}\mid\Delta_{||}=0,\Delta_\perp,\Delta'=0)\cdot\underline{\Delta}^{-1}(\mathbf{k}\mid\Delta_{||},\Delta_\perp,\Delta'=0)] \ . \tag{2.19b}$$

It is then easy to see that

$$a_{||}+a_\perp=\frac{2}{NZ}\sum_{\mathbf{k}}\mathrm{Tr}[\underline{\Delta}(\mathbf{k}\mid\Delta_{||},\Delta_\perp,\Delta'=0)\cdot\underline{\Delta}^{-1}(\mathbf{k}\mid\Delta_{||},\Delta_\perp,\Delta'=0)]=\frac{6}{Z} \ , \tag{2.20}$$

where the Tr symbol indicates a 3×3 trace operation. This then leads to

$$p^*=a_{||}^*=a_\perp^*=\frac{3}{Z} \ , \tag{2.21}$$

which again agrees with the estimate of the constraint argument.

(ii) $D'\neq0$. In this case there are three self-consistency equations. The structure of the first two is again the same as that of Eqs. (2.14). The third condition is

$$\frac{\Delta'}{D'}=\frac{p-a'}{1-a'} \ . \tag{2.22}$$

The quantities $a_{||}$, $a_\perp$, and a' are defined as

$$a_{||}=\frac{2}{NZ}\sum_{\mathbf{k}}\mathrm{Tr}[\underline{\Delta}(\mathbf{k}\mid\Delta_{||},\Delta_\perp=0,\Delta'=0)\cdot\underline{\Delta}^{-1}(\mathbf{k}\mid\Delta_{||},\Delta_\perp,\Delta')] \ , \tag{2.23a}$$

$$a_\perp=\frac{2}{NZ}\sum_{\mathbf{k}}\mathrm{Tr}[\underline{\Delta}(\mathbf{k}\mid\Delta_{||}=0,\Delta_\perp,\Delta'=0)\cdot\underline{\Delta}^{-1}(\mathbf{k}\mid\Delta_{||},\Delta_\perp,\Delta')] \ , \tag{2.23b}$$

and

$$a'=\frac{2}{NZ}\sum_{\mathbf{k}}\mathrm{Tr}[\underline{\Delta}(\mathbf{k}\mid\Delta_{||}=0,\Delta_\perp=0,\Delta')\cdot\underline{\Delta}^{-1}(\mathbf{k}\mid\Delta_{||},\Delta_\perp,\Delta')] \ . \tag{2.23c}$$

In this case

$$a_{||}+a_\perp+a'=\frac{2}{NZ}\sum_{\mathbf{k}}\mathrm{Tr}[\underline{\Delta}(\mathbf{k}\mid\Delta_{||},\Delta_\perp,\Delta')\cdot\underline{\Delta}^{-1}(\mathbf{k}\mid\Delta_{||},\Delta_\perp,\Delta')]=\frac{6}{Z} \ , \tag{2.24}$$

and we find

$$p^*=a_{||}^*=a_\perp^*=(a')^*=\frac{2}{Z} \ . \tag{2.25}$$

This is the same as the Born-model geometrical percolation limit which again agrees with the constraint estimate.

b. Dynamic approach. The above equations can also be derived from a multiple-scattering viewpoint. In this case we picture a wave propagating through an effective medium and incident upon a selected bond (say i—j). This bond can either be present (probability p) or absent (probability $1-p$) and the effective medium is determined by requiring that the average scattering vanish. To illustrate the form of these arguments, we consider the Born model. The scattering operators that describe the distinguished bond are of the following forms: *bond present,*

$$T^{(1)}=[T_{||}^{(1)}\hat{\mathbf{R}}_{ij}\hat{\mathbf{R}}_{ij}+T_\perp^{(1)}(\underline{1}-\hat{\mathbf{R}}_{ij}\hat{\mathbf{R}}_{ij})]\begin{bmatrix}1&-1\\-1&1\end{bmatrix} \ , \tag{2.26a}$$

and *bond missing,*

$$T^{(2)}=[T_{||}^{(2)}\hat{\mathbf{R}}_{ij}\hat{\mathbf{R}}_{ij}+T_\perp^{(2)}(\underline{1}-\hat{\mathbf{R}}_{ij}\hat{\mathbf{R}}_{ij})]\begin{bmatrix}1&-1\\-1&1\end{bmatrix} \ . \tag{2.26b}$$

where

$$T_{||(\perp)}^{(1)}=\frac{D_{||(\perp)}-\Delta_{||(\perp)}}{1+(D_{||(\perp)}-\Delta_{||(\perp)})(G_{||(\perp)}-G_0)} \tag{2.27a}$$

and

$$T^{(2)}_{||(\perp)}=\frac{-\Delta_{||(\perp)}}{1-\Delta_{||(\perp)}[G_{||(\perp)}-G_0]} . \tag{2.27b}$$

Here the quantities G_0 and $G_{||(\perp)}$ are defined in terms of the resolvent matrix

$$G(\mathbf{R}_n \mid \omega^2)=\frac{1}{N}\sum_{\mathbf{k}}\frac{e^{i\mathbf{k}\cdot\mathbf{R}_n}}{\omega^2-\Delta(\mathbf{k})} , \tag{2.28}$$

where $\Delta(\mathbf{k})$ is the matrix defined in Eq. (2.12). In the $\mathbf{R}_n=0$ case, this matrix is isotropic, i.e.,

$$G(\mathbf{R}_n \mid \omega^2)\to G_0(\omega^2)\mathbb{1} .$$

If $\mathbf{R}_n$ is one of the nearest-neighbor vectors, we have

$$G(\mathbf{R}_n \mid \omega^2)=G_{||}(\omega^2)\hat{\mathbf{R}}_n\hat{\mathbf{R}}_n+G_\perp(\omega^2)(\mathbb{1}-\hat{\mathbf{R}}_n\hat{\mathbf{R}}_n) . \tag{2.29}$$

As we are interested primarily in long-wavelength behavior, we will be concerned with the limit $\omega^2\to 0$. Thus the quantities entering Eq. (2.27) are defined as $G_0\equiv G_0(\omega^2\to 0)$, $G_{||}\equiv G_{||}(\omega^2\to 0)$, and $G_\perp\equiv G_\perp(\omega^2\to 0)$. The equations defining $\Delta_{||}$ and $\Delta_\perp$ are then

$$pT_{||(\perp)}+(1-p)T_{||(\perp)}=0 . \tag{2.30}$$

These equations are easily rewritten as

$$\frac{pD_{||(\perp)}-\Delta_{||(\perp)}}{D_{||(\perp)}-\Delta_{||(\perp)}}=2\Delta_{||(\perp)}(G_{||(\perp)}-G_0)=a_{||(\perp)} , \tag{2.31}$$

which are clearly identical to the results (2.14) obtained by the static arguments presented above. [The last equality in (2.31) can be verified by combining Eqs. (2.28) with (2.11) and (2.15).] It is clear that the above analysis can easily be extended to the disk models and, with relatively little effort, one finds that Eqs. (2.19)–(2.25) can be derived by the dynamic approach.

c. Numerical results. In Figs. 3–5 calculations based on effective-medium theory and numerical simulation are compared for the Born model. It is clear that in this case the agreement between the two methods is very good. We see that a threshold is reached very close to the mean-field prediction $p^*=\frac{1}{3}$, and that the ratio $K/\mu\to 1$ as $p\to p^*$.

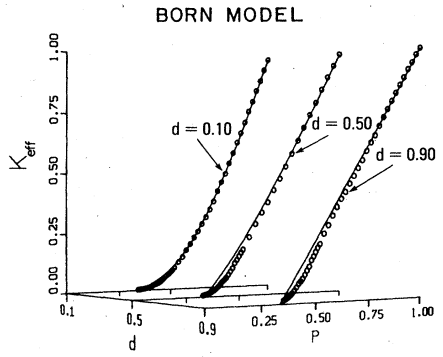

FIG. 3. Effective medium (solid curves) and computer simulation (open circles) are compared for the bulk modulus of the Born model. Here $d\equiv D_\perp/D_{||}$ indicates the relative strength of the transverse coupling.

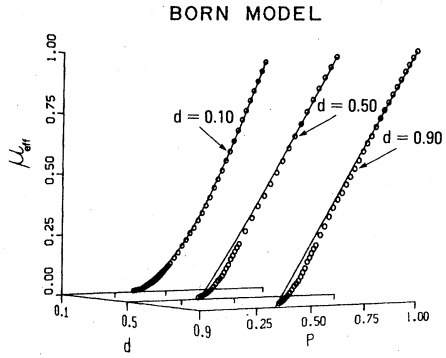

FIG. 4. Effective medium (solid curves) and computer simulation (open circles) are compared for the shear modulus of the Born model.

It can easily be shown that the effective-medium equations (2.14) lead to *isotropic* behavior at the depletion transition (i.e., $K\to\mu$ as $p\to p_c^*$). This isotropy means that the x and y problems decouple and we have two scalar problems. Because the Born model is not rotationally invariant, some care must be taken in deriving K and μ from $\Delta_{||}$ and $\Delta_\perp$. In particular, one must ensure (as in Fig. 1) that the applied strains have no rotational component. The correct relations are then

$$K=\frac{\sqrt{3}}{2}\Delta_{||},\quad \mu=\frac{\sqrt{3}}{4}(\Delta_{||}+\Delta_\perp) . \tag{2.32}$$

Note that in Figs. 3 and 4 the results obtained by simulation are systematically below those obtained by effective-medium theory in the range $p_c^*\le p\le 0.5$. Nevertheless, the level of agreement in the flow diagram (Fig. 5) is excellent.

In Figs. 6–8 corresponding results are shown for the disk model in the special case $D'=0$. Here the agreement is somewhat less satisfactory. It is clear that the behavior

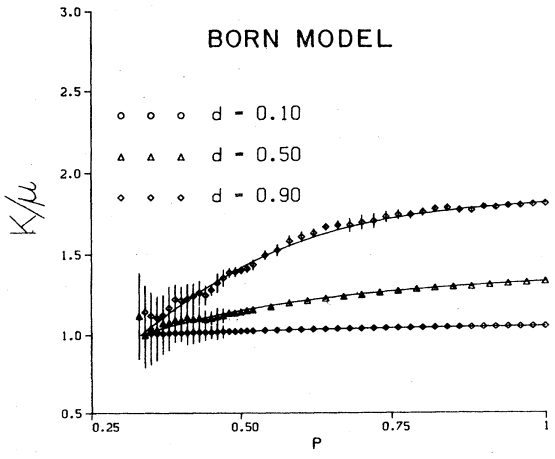

FIG. 5. Effective medium (solid curves) and computer simulation (open circles) are compared for the ratio of the bulk to shear modulus of the Born model. The vertical bars represent statistical errors associated with the number of independent realizations simulated.

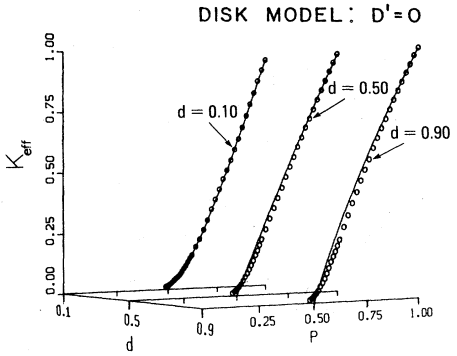

FIG. 6. Effective medium (solid curves) and computer simulation (open circles) are compared for the bulk modulus of the $D'=0$ disk model. Here $d \equiv D_\perp / D_{||}$ indicates the relative strength of the transverse coupling.

of K and μ as a function of p is represented in a reasonable way by the effective-medium equations. In addition, these equations predict that the ratio K/μ should approach a fixed point at the transition. We see, however, that the value of this ratio is not given properly by effective-medium theory. In this connection we note that the present results do *not* appear to be consistent with the Bergman-Kantor[2] conjecture $K/\mu \to 2/d$ (d is the spatial dimension). In Figs. 9—11 we see that a similar situation obtains in the case of nonvanishing D'. Here the simulations indicate that K/μ approaches a value that is consistent with the Bergman-Kantor value (2.0). (In the present case, the uncertainty in our simulation results reflects *systematic* errors associated with finite-size effects rather than *statistical* errors, whose magnitude is indicated by the vertical bars.) Note that in both cases the value of the transition obtained in the disk model is in excellent agreement with the constraint-counting results.

D. Bond-bending (second-neighbor) models

In Figs. 12—14 we show the results of numerical simulations on the bond-bending model. The transition takes place at $p = p_c^{(\mathrm{cond})}$ as expected, and the limiting value of

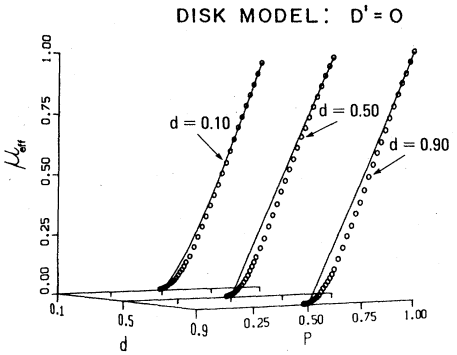

FIG. 7. Effective medium (solid curves) and computer simulation (open circles) are compared for the shear modulus of the $D'=0$ disk model.

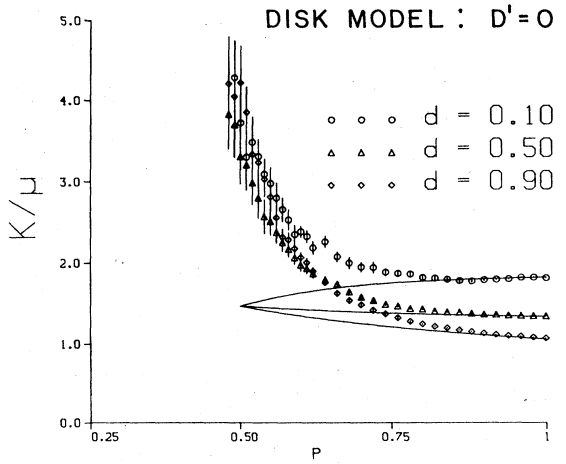

FIG. 8. Effective medium (solid curves) and computer simulation (open circles) are compared for the ratio of the bulk to shear modulus of the $D'=0$ disk model. The vertical bars represent *statistical* errors associated with the number of independent realizations simulated.

K/μ is again consistent with the Bergman-Kantor value 2.0. While it is possible to derive effective-medium equations by generalizing the static arguments presented above,[29] they yield neither the proper slope as $p \to 1$ nor do they give the expected value for the transition point (i.e., $p^* = \frac{1}{3}$). Finally, we note that because bond-bending forces couple three particles (and six degrees of freedom), there is no clearcut way to generalize the dynamic (i.e., scattering) derivations of effective-medium theory.

III. CONTINUUM MODELS

Effective-medium theories for the continuum case are set up in the same spirit as those for the discrete case.[10—13] We consider the case of elliptical holes cut randomly in an isotropic two-dimensional elastic continuum. The major and minor semiaxes of the ellipses are a and b. (By convention, we take $b \leq a$.) The centers and axes of the ellipses are randomly positioned in the plane and, of

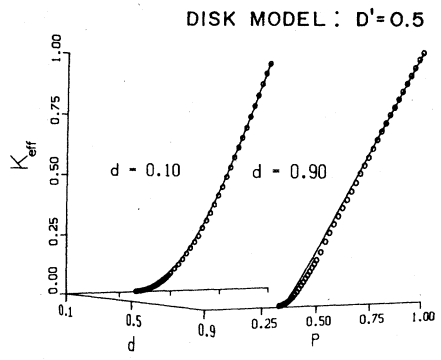

FIG. 9. Effective medium (solid curves) and computer simulation (open circles) are compared for the bulk modulus of the $D'=0.5$ disk model. Here $d \equiv D_\perp / D_{||}$ indicates the relative strength of the transverse coupling.

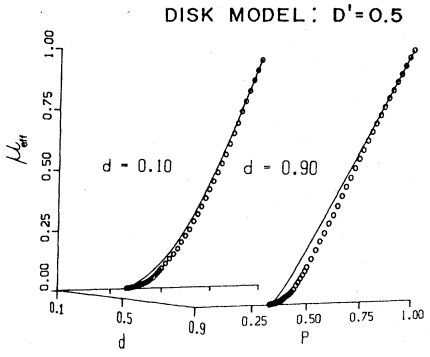

FIG. 10. Effective medium (solid curves) and computer simulation (open circles) are compared for the shear modulus of the $D'=0.5$ disk model.

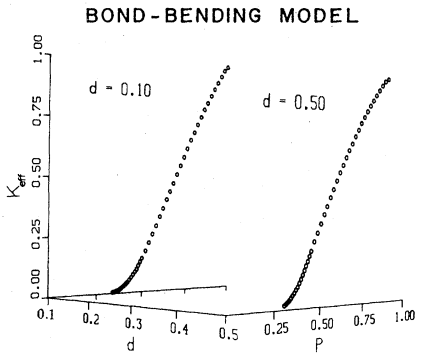

FIG. 12. Computer-simulation results are shown for bulk modulus in the bond-bending model. Here $d \equiv D_\perp / D_{||}$ indicates the relative strength of the transverse coupling.

course, the ellipses can overlap one another. The reason for choosing ellipses (rather than say rectangles) is that the problem of a *single* elliptical inclusion can be solved exactly. The effective-medium theory then uses this exact result for one inclusion to derive approximate results for many inclusions.

Two distinct self-consistent effective-medium approximations have been discussed in the literature.[10] In the first, the host and the inclusions are treated *symmetrically*. We refer to this as SCA-S. In the second (referred to as SCA-A) the host and the inclusions are treated *asymmetrically*. In this respect the continuum situation is rather different from the lattice cases discussed in Sec. II. There, both the cut and uncut bonds have the same "shape," so that it is natural to average symmetrically over the scattering operators that describe the two possibilities. By contrast, in the case of elliptical holes in a continuum, the host and the inclusions are manifestly different and, indeed, the SCA-A is generally to be preferred to the SCA-S.

Disordered two-dimensional elastic systems are characterized by the elastic constants $K_{\rm eff}$ and $\mu_{\rm eff}$. These quantities are functions of the volume fraction of the holes, $1-p$, and their aspect ratio, b/a. Effective-medium theories do not treat overlap effects between different ellipses explicitly. If there are n ellipses per unit area, then the volume fraction p occupied by the background material is[30]

$$p = e^{-(n\pi ab)} . \tag{3.1}$$

For small n, $p \sim 1 - n\pi ab$ as expected, but the corrections are very important for larger values of n. For circles at percolation,[31,32] $n_c \pi ab = 1.1 \pm 0.05$ and $p_c = 0.33 \pm 0.02$. For high-aspect-ratio (i.e., needlelike) ellipses, the corrections for overlap are less important (than for circles) and $p_c \to 1$ as $b/a \to 0$. It is the volume fraction p given in (3.1) that enters the effective-medium theories.

We now briefly recall the salient formulas for the continuum EMA.[13] The key invariant quantities needed when an isotropic average is done over all directions in two dimensions are

$$P = \tfrac{1}{2} \sum_{i,j} T_{iijj}, \quad Q = \tfrac{1}{2} \sum_{i,j} (T_{ijij} - \tfrac{1}{2} T_{iijj}) . \tag{3.2}$$

Here T_{ijkl} is the tensor which relates homogeneous strains outside the inclusion to those inside. In general, P and Q depend on shape of the inclusion and the moduli of both the inclusion and the host. The general expressions can be

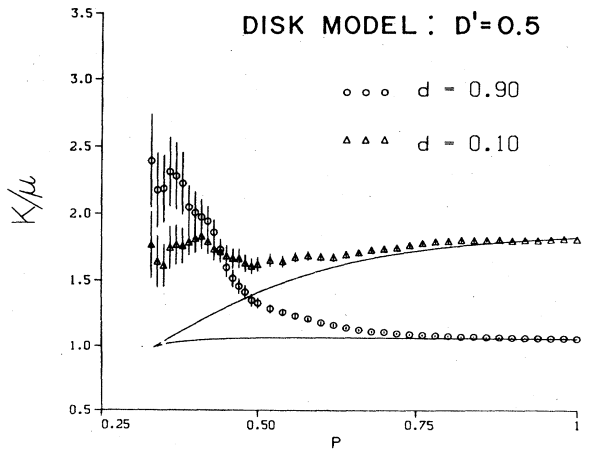

FIG. 11. Effective medium (solid curves) and computer simulation (open circles) are compared for the ratio of the bulk to shear modulus of the $D'=0.5$ disk model. The vertical bars represent *statistical* errors associated with the number of independent realizations simulated.

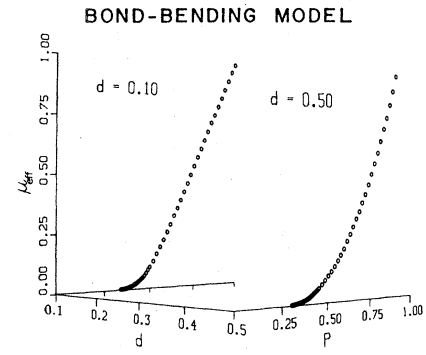

FIG. 13. Computer-simulation results are shown for the shear modulus in the bond-bending model.

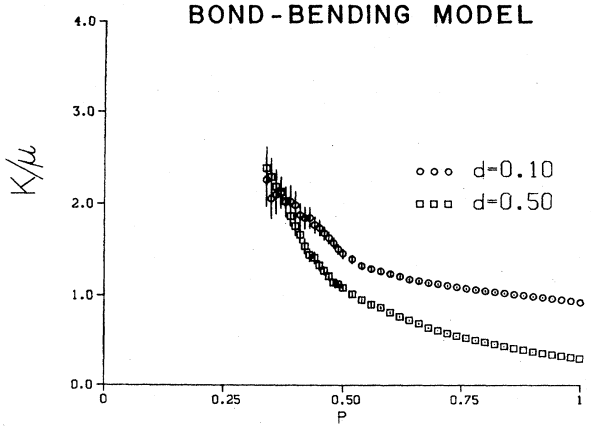

FIG. 14. Computer-simulation results are shown for the ratio of the bulk to shear modulus of the bond-bending model. The vertical bars represent *statistical* errors associated with the number of independent realizations simulated.

found in Ref. 13. Two cases of interest, namely circles and needles, are given in Table III.

Consider first the symmetric effective-medium theory, which treats the host and the inclusions symmetrically. It leads to equations of the form[13]

$$\sum_i c_i P_{\rm eff}^{(i)}(K_{\rm eff}-K_i)=0, \quad \sum_i c_i Q_{\rm eff}^{(i)}(\mu_{\rm eff}-\mu_i)=0 , \tag{3.3}$$

where the sum on i runs over the two constituents. In the case of interest here, the second constituent (i.e., the randomly oriented elliptical holes) has $K_i=0$ and $\mu_i=0$, and Eqs. (3.3) reduce to

$$\frac{K_{\rm eff}}{K_1}=\frac{1-\alpha/p}{1-\alpha}, \quad \frac{\mu_{\rm eff}}{\mu_1}=\frac{1-\beta/p}{1-\beta} , \tag{3.4}$$

where

$$\alpha=(1-P_{\rm eff}^{(1)}/P_{\rm eff}^{(2)})^{-1}, \quad \beta=(1-Q_{\rm eff}^{(1)}/Q_{\rm eff}^{(2)})^{-1} . \tag{3.5}$$

It can be shown that the SCA-S gives the following expression for the percolation threshold:

$$p^*=2\{1+[2(a+b)^2/(a^2+b^2)]^{1/2}\}^{-1} . \tag{3.6}$$

Next consider the asymmetric self-consistent approximation. The SCA-A leads to the general equations[13]

$$\frac{1}{K_{\rm eff}}=\frac{1}{K_1}\left[1+\sum_i (1-p_i)P_{\rm eff}^{(i)}\left[\frac{K_1-K_i}{K_{\rm eff}}\right]\right] , \tag{3.7a}$$

TABLE III. Limiting forms of P and Q [defined in Eq. (3.2)] for circle- and needle-shaped inclusions. K (K_1) and μ (μ_1) refer to the host (inclusion), respectively.

	P	Q
Circle	$\frac{K+\mu}{K_1+\mu}$	$\frac{2(K+\mu)\mu}{K\mu+(K+2\mu)\mu_1}$
Needle	$\frac{K+\mu_1}{K_1+\mu_1}$	$\frac{1}{2}\left[\frac{K_1+\mu}{K_1+\mu_1}+\frac{\mu}{\mu_1}\right]$

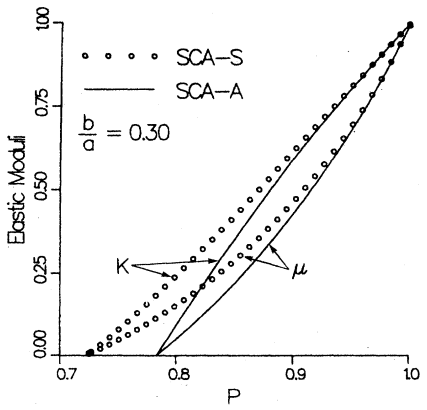

FIG. 15. K and μ are shown as a function of p for the two continuum effective-medium theories.

and

$$\frac{1}{\mu_{\rm eff}}=\frac{1}{\mu_1}\left[1+\sum_i (1-p_i)Q_{\rm eff}^{(i)}\left[\frac{\mu_1-\mu_i}{\mu_{\rm eff}}\right]\right] . \tag{3.7b}$$

Here we have taken material 1 as a host. Again assuming that the inclusions have $K_2=0$ and $\mu_2=0$, we find

$$\frac{K_{\rm eff}}{K_1}=\frac{p-\alpha}{1-\alpha}, \quad \frac{\mu_{\rm eff}}{\mu_1}=\frac{p-\beta}{1-\beta} , \tag{3.8}$$

where $\alpha=1-1/P_{\rm eff}$ and $\beta=1-1/Q_{\rm eff}$. In this approach the expression for the threshold is

$$p^*=[1+ab/(a^2+b^2)]^{-1} . \tag{3.9}$$

Illustrative calculations based on SCA-S and SCA-A are presented in Figs. 15 and 16. In Fig. 15 we plot $K_{\rm eff}$ and $\mu_{\rm eff}$ obtained from Eqs. (3.3) and (3.7), respectively. In Fig. 16 results are shown for p^* based on Eqs. (3.6) and (3.9). *Both* approaches lead to the result

$$p^*+\sigma^*=1 , \tag{3.10}$$

where σ^* is the value of the Poisson ratio at percolation,

$$\sigma^*=\frac{K^*-\mu^*}{K^*+\mu^*}=\frac{K^*/\mu^*-1}{K^*/\mu^*+1} . \tag{3.11}$$

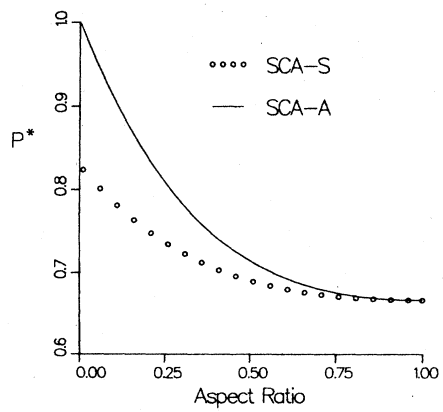

FIG. 16. p^* is shown as a function of the aspect ratio of the ellipse for the two continuum mean-field theories.

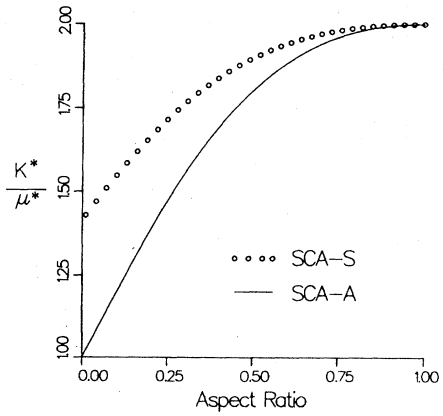

FIG. 17. The ratio K^*/μ^* at the transition point p^* is shown as a function of the aspect ratio of the ellipse for the two continuum mean-field theories.

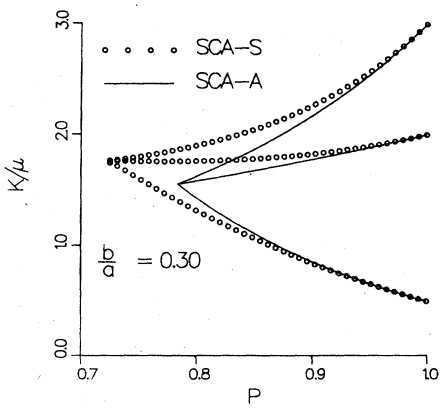

FIG. 18. K/μ is shown as a function of p for the two continuum mean-field theories.

Here K^* (μ^*) are the values of the bulk (shear) modulus at the transition point. (Both K^* and μ^* approach zero as $p \to p^*$; their ratio, however, remains finite.) The value of p^* and hence those of σ^* and K^*/μ^* depend on the geometries but not on the initial value of K/μ. Thus the continuum model has a fixed point within effective-medium theory and one expects that numerical simulations will eventually yield corresponding behavior. The ratio of the longitudinal to transverse sound velocities is given by

$$\frac{V_L^2}{V_T^2} = 1 + \frac{K}{\mu} . \tag{3.12}$$

At the transition point this becomes

$$\left[\frac{V_L^2}{V_T^2}\right]^* = 1 + \frac{K^*}{\mu^*} = \frac{2}{p^*} . \tag{3.13}$$

It is curious that both approaches lead to (3.10) even though the p^* (and hence σ^*) are rather different (see Fig. 15). For circles both effective-medium theories are identical, but then they differ for general ellipses as shown in Fig. 16. In Fig. 17 we show the values of K^*/μ^* at the fixed point as a function of the aspect ratio of the elliptical inclusions. For a fixed aspect ratio, flow to the fixed point is illustrated in Fig. 18. It follows from Eqs. (3.6), (3.9), and (3.10) that at the fixed points we have

$$\frac{K^*}{\mu^*} = \left[\frac{2(a+b)^2}{a^2+b^2}\right]^{1/2} \quad \text{(SCA-S)} \tag{3.14a}$$

and

$$\frac{K^*}{\mu^*} = \frac{(a+b)^2}{a^2+b^2} \quad \text{(SCA-A)} . \tag{3.14b}$$

IV. CONCLUSIONS

The elastic depletion transition has been studied for a variety of models with transverse forces. In the case of systems with nearest-neighbor forces we find that the agreement between computer simulations and effective-medium theory is quite good over the entire (p) range of interest. In these systems effective-medium theory and constraint-counting arguments yield the same results for p^* and this estimate agrees with the p_c^* obtained by simulation to within about 1%. The results obtained here are consistent with those presented in Refs. 15 (triangular lattice, nearest-neighbor central forces) and 19 (square lattice, first- and second-neighbor central forces). The only differences between these systems are in the deviations between the effective-medium theory and the numerical results in the region above p_c^*. These deviations are least pronounced in the central-force case and are more substantial for the models discussed in this paper. In addition, we note that the effective-medium flow diagrams are quantitatively accurate only in the case of the point-mass models. We have no physical argument that would predict this state of affairs. Nevertheless, we believe that the present work provides further evidence that fixed points and flow diagrams are useful in discussing the elastic depletion transition.

ACKNOWLEDGMENT

One of us (M.F.T.) would like to thank the National Science Foundation, the Office of Naval Research, and Schlumberger-Doll Research for support during the course of this research.

*Present address: Physics Department, Harvard University, Cambridge, MA 02138.

†Permanent address: Department of Physics and Astronomy, Michigan State University, East Lansing, MI 49824.

[1]S. Feng and P. N. Sen, Phys. Rev. Lett. **52**, 216 (1984).

[2]D. Bergman and Y. Kantor, Phys. Rev. Lett. **53**, 511 (1984).

[3]Y. Kantor and I. Webman, Phys. Rev. Lett. **52**, 1891 (1984).

[4]S. Feng, P. N. Sen B. I. Halperin, and C. J. Lobb, Phys. Rev. B **30**, 5386 (1984).

[5]D. Bergman Phys. Rev. B **31**, 1696 (1985).

[6]B. I. Halperin, S. Feng, and P. N. Sen, Phys. Rev. Lett. **54**, 2391 (1985).

[7]S. Alexander, J. Phys. (Paris) **45**, 1939 (1984).
[8]M. F. Thorpe, J. Non-Cryst. Solids **57**, 355 (1983).
[9]M. Sahimi, B. D. Hughes, L. E. Scriven, and H. T. Davis, J. Chem. Phys. **78**, 6849 (1983).
[10]J. Berryman, J. Acous. Soc. Am. **68**, 1820 (1980).
[11]T. T. Wu, Int. J. Solids Struct. **3**, 1 (1966); R. Hill, J. Mech. Phys. Solids **13**, 213 (1965); B. Budiansky, *ibid.* **13**, 223 (1965).
[12]J. D. Eshelby, Proc. R. Soc. London, Ser. A **241**, 376 (1957).
[13]M. F. Thorpe and P. N. Sen, J. Acoust. Soc. Am. **77**, 1674 (1985).
[14]L. Benguigui, Phys. Rev. Lett. **53**, 2028 (1984) [see also P. N. Sen and M. F. Thorpe, *ibid.* **54**, 1463; L. Benguigui, *ibid.* **54**, 1464 (1985)]; D. Deptuck, J. P. Harrison, and P. Zawadzki, *ibid.* **54**, 913 (1985).
[15]S. Feng, M. F. Thorpe, and E. J. Garboczi, Phys. Rev. B **31**, 276 (1985).
[16]M. A. Lemieux, P. Breton, and A. M. S. Tremblay, J. Phys. (Paris) Lett. **46**, L1 (1985).
[17]G. S. Grest and I. Webman, J. Phys. (Paris) Lett. **45**, 1155 (1984); I. Webman and G. S. Grest, Phys. Rev. B **31**, 1689 (1985).
[18]E. J. Garboczi and M. F. Thorpe, Phys. Rev. B **31**, 7276 (1985).
[19]H. He and M. F. Thorpe, Phys. Rev. Lett. **54**, 2107 (1985).
[20]S. Feng Phys. Rev. B **32**, 510 (1985).
[21]J. G. Kirkwood, J. Chem. Phys. **7**, 506 (1939).
[22]P. N. Keating, Phys. Rev. **145**, 637 (1966).
[23]L. M. Schwartz, D. L. Johnson, and S. Feng, Phys. Rev. Lett. **52**, 831 (1984).
[24]S. Kirkpatrick, Rev. Mod. Phys. **45**, 574 (1973).
[25]For a review, see R. J. Elliott, J. A. Krumhansl, and P. L. Leath, Rev. Mod. Phys. **46**, 465 (1974).
[26]M. Born and K. Huang, *Dynamical Theory of Crystal Lattices* (Oxford University Press, New York, 1954).
[27]L. A. Hageman and D. M. Young, *Applied Iterative Methods* (Academic, New York, 1981); see also E. S. Kirkpatrick, Phys. Rev. Lett. **27**, 1722 (1971).
[28]For a given value of p, calculations carried out on the 40×40 lattice differed from those carried out on the 30×30 lattice by no more than 3% or 4%. The reduction in systematic errors associated with the larger lattice was not great enough to significantly change any of the results presented in this paper.
[29]S. Feng and L. Schwartz (unpublished).
[30]S. A. Roach [in *The Theory of Random Clumping* (Meuthen, London, 1968)] has shown this formula to be true for circles (see p. 57). It can easily be extended to ellipses [M. F. Thorpe (unpublished)].
[31]D. H. Fremlin, J. Phys. (Paris) **37**, 813 (1976).
[32]E. T. Gwalinsky and H. E. Stanley, J. Phys. A **14**, L291 (1981).